AGU ADVANCING EARTH AND SPACE SCIENCE

Geophysical Research Letters

RESEARCH LETTER
10.1029/2020GL088692

Late 20th Century Indian Ocean Heat Content Gain Masked by Wind Forcing

Caroline C. Ummenhofer[1,2], Svenja Ryan[1], Matthew H. England[2,3], Markus Scheinert[4], Patrick Wagner[4], Arne Biastoch[4,5], and Claus W. Böning[4,5]

[1]Department of Physical Oceanography, Woods Hole Oceanographic Institution, Woods Hole, MA, USA, [2]ARC Centre of Excellence for Climate Extremes, University of New South Wales, Sydney, NSW, Australia, [3]Climate Change Research Centre, University of New South Wales, Sydney, NSW, Australia, [4]GEOMAR Helmholtz Centre Ocean Research Kiel, Kiel, Germany, [5]Faculty of Mathematics and Natural Sciences, Christian-Albrechts University, Kiel, Germany

Key Points:
- Multidecadal variations in Indian Ocean heat content exhibit distinct spatiotemporal signals regionally and with depth
- Winds counteracted (western) Indian Ocean heat content increase due to buoyancy forcing prior to the 2000s but contributed to the rapid rise since
- Progressive shoaling of the Indian Ocean thermocline appears to be dominated by multidecadal variation in wind forcing

Supporting Information:
- Supporting Information S1

Correspondence to:
C. C. Ummenhofer,
cummenhofer@whoi.edu

Citation:
Ummenhofer, C. C., Ryan, S., England, M. H., Scheinert, M., Wagner, P., Biastoch, A., & Böning, C. W. (2020). Late 20th century Indian Ocean heat content gain masked by wind forcing. *Geophysical Research Letters*, *47*, e2020GL088692. https://doi.org/10.1029/2020GL088692

Received 1 MAY 2020
Accepted 28 SEP 2020
Accepted article online 26 OCT 2020

Abstract Rapid increases in upper 700-m Indian Ocean heat content (IOHC) since the 2000s have focused attention on its role during the recent global surface warming hiatus. Here, we use ocean model simulations to assess distinct multidecadal IOHC variations since the 1960s and explore the relative contributions from wind stress and buoyancy forcing regionally and with depth. Multidecadal wind forcing counteracted IOHC increases due to buoyancy forcing from the 1960s to the 1990s. Wind and buoyancy forcing contribute positively since the mid-2000s, accounting for the drastic IOHC change. Distinct timing and structure of upper ocean temperature changes in the eastern and western Indian Ocean are linked to the pathway how multidecadal wind forcing associated with the Interdecadal Pacific Oscillation is transmitted and affects IOHC through local and remote winds. Progressive shoaling of the equatorial thermocline—of importance for low-frequency variations in Indian Ocean Dipole occurrence—appears to be dominated by multidecadal variations in wind forcing.

Plain Language Summary Indian Ocean surface waters have warmed more than the tropical Atlantic or Pacific over the last 60 years. In contrast, the amount of heat stored in the upper 700 m of the Indian Ocean did not exhibit strong increases between 1960 and 2000, which is counter to temperature trends in other ocean regions across the globe. Only since the 2000s was rapid warming down to 700 m observed for the Indian Ocean. Using ocean model simulations, our study demonstrates that the unusual behavior of Indian Ocean temperatures over the last 60 years was mainly due to wind conditions: Two different pathways how winds can impact the upper ocean temperature structure in the Indian Ocean, either through the atmosphere or via an oceanic connection from the Pacific, are highlighted. In fact, wind trends during 1960–2000 counteracted additional heat input into the Indian Ocean due to an overall warming climate. These long-term changes in the Indian Ocean temperature structure affect regional climate in surrounding countries; they are also of importance for predicting how the Indian Ocean will respond in the near future to a warming climate.

1. Introduction

Superimposed on a long-term warming trend, global mean surface temperatures exhibit a high level of variability, including periods of relatively low or near-zero warming, such as the *hiatus* period at the start of the 21st century. There is an emerging consensus that continued ocean warming and reorganization of oceanic heat content (OHC) during that time stalled surface temperature increases (Bindoff et al., 2019). Over the sustained La Niña-like period during the years 2000–2015 associated with the negative phase of the Interdecadal Pacific Oscillation (IPO), the Pacific surface was cool but with little concomitant increase in tropical upper OHC (e.g., England et al., 2014; Kosaka & Xie, 2013). Instead, subsurface heat buildup in the Indian Ocean seems to have played a role (Vialard, 2015), both through regional surface warming (Luo et al., 2012) and heat redistributed from the neighboring Pacific through the Indonesian Archipelago (e.g., Lee et al., 2015; Nieves et al., 2015). Indeed, Lee et al. (2015) suggested that OHC in the Indian Ocean (IOHC) could account for >70% of the global upper 700-m OHC gain during the past decade, though later estimates have challenged these numbers (e.g., Cheng et al., 2017). The exact contributions from different pathways of heat transfer from the Pacific to Indian Ocean remain unclear, i.e., via the atmosphere, via the ocean, or some combination of the two most likely (e.g., Jin, Kwon, Ummenhofer, Seo, Schwarzkopf,

et al., 2018). Partitioning between different pathways has implications for the emergence of OHC anomalies in the Indian Ocean with regard to timing and location of OHC changes within the ocean basin. Furthermore, questions remain how variability at the multidecadal timescale may act to modulate or even mask long-term (anthropogenic) heat gains in the Indian Ocean. Here, we use eddy-active ocean model experiments to address these questions about upper ocean temperature changes in the Indian Ocean on multidecadal timescales and their implications for the basin's thermocline structure.

Several studies focused on the rapid warming observed in the southern Indian Ocean in recent decades: Li et al. (2017) identified a "hot spot" with warming rates of 0.8–1.2°C/decade during the period 2003–2012 in the southeast Indian Ocean (90–125°E, 5–36°S) that accounted for more than half of the upper IOHC gain. They attributed this mainly to strengthened Pacific trade winds and Indonesian Throughflow (ITF) during the negative IPO phase, yet suggested that anthropogenic forcing could have amplified this warming compared to earlier IPO phase transitions. Zhang et al. (2018) attributed a warming rate of 0.013°C/year for the upper 700 m in the South Indian Ocean during 1998–2015 predominantly to decreased cooling from net air-sea heat flux and warming due to heat advection from a strengthened ITF. Using historic data, Li et al. (2020) found 70% of subsurface warming signals in the Indian Ocean to be associated with warming/cooling near 100 m and 21% with a basin-wide dipole mode between the surface (<60-m depth) and the 60- to 400-m depth range, with the dipole predominantly associated with ITF variability.

Direct observational evidence of ITF transport trends is scarce, especially for multidecadal timescales that allow placing the trends post-2000 into a long-term context. Liu et al. (2015) observed a strengthening ITF trend of 1 Sv/decade in the repeated expendable bathythermograph (XBT) line between Fremantle (Western Australia) and Sunda Strait (Indonesia) during 1984–2013, though caution that decadal variability needs to be considered when calculating ITF from geostrophic transport using XBT. Furthermore, whether increased ITF transport necessarily scales with increased heat advection is less clear, as total volume transport does not reflect the relative contributions of the warm upper and cool lower layers. Gruenburg and Gordon (2018) found southward heat advection through Makassar Strait to increase rapidly during 2006–2008, peaking in 2008–2009, but decreasing afterwards to a minimum in 2015.

Beyond the recent rapid warming of IOHC and the role of heat advection through the ITF driven by strengthened equatorial Pacific winds during the negative IPO phase, several studies explored the role of Pacific climate variability for upper ocean properties in the Indian Ocean over the past 50 years more broadly. Schwarzkopf and Böning (2011) attributed multidecadal changes in Indian Ocean sea surface height, including a pronounced downward trend during the 1960s to the 2000s, concomitant subsurface cooling, and a shoaling thermocline, to Pacific wind forcing associated with the Pacific Decadal Oscillation. In regional HYCOM simulations, Trenary and Han (2013) found decadal sea level and subsurface temperature variations in the southern Indian Ocean to be due to vertical thermocline displacements forced by equatorial Pacific trade winds since the 1990s. Investigating IOHC changes in the upper 400 m, Li et al. (2018) attributed rapid Indian Ocean warming (cooling) periods during 1965–1979 (1980–96) to strengthened (weakened) Pacific trade winds and ITF transport during negative (positive) IPO phases. However, they found that post-2000, the rapid IOHC warming was rather driven by wind and heat flux forcing within the Indian Ocean, dominated by easterly wind trends in the equatorial Indian Ocean and Ekman downwelling off equator (Li et al., 2018). In contrast, Maher et al. (2018) found that a substantial component of IOHC evolution during 1992–2011 could be explained by forced ITF variations due to the unprecedented trade wind acceleration in the Pacific. Given that both heat fluxes and ocean heat advection seem to contribute to the decadal IOHC response, this raises the question where, both spatially and with depth, the signal emerges within the Indian Ocean. Furthermore, what is the relative contribution of different pathways (oceanic vs. atmospheric) how IPO-related forcing from the Pacific is transmitted to the Indian Ocean?

The IPO enhances (weakens) external forcing over the Indian Ocean by 50% during IPO warm (cold) phases, accounting for 10% of the global warming hiatus post-1999, with the signal affecting decadal Indian Ocean sea surface temperature (SST) variability transmitted via atmospheric adjustment through changing surface heat fluxes and thermocline depth (Dong et al., 2016). Focusing on decadal subsurface IOHC instead, Jin, Kwon, Ummenhofer, Seo, Schwarzkopf, et al. (2018) and Jin, Kwon, Ummenhofer, Seo, Kosaka, et al. (2018) found distinct mechanisms for IPO-related Pacific forcing to be transmitted to the Indian Ocean in the east and west of the basin: an oceanic pathway, where eastern subsurface IOHC is predominantly driven by

western Pacific surface wind variations triggering oceanic Rossby waves, propagating through the Indonesian Seas and influencing ITF heat transport; in contrast, decadal western Indian Ocean IOHC variations are primarily due to oceanic Rossby waves triggered by anomalous wind stress curl and Ekman pumping in the central Indian Ocean induced by a remote atmospheric response to Pacific IPO-forcing through the zonal Walker circulation (Jin, Kwon, Ummenhofer, Seo, Schwarzkopf, et al., 2018; Jin, Kwon, Ummenhofer, Seo, Kosaka, et al., 2018). Here, we further disentangle the role of different atmospheric factors for IOHC changes, namely, by looking at the relative contribution of buoyancy and wind stress forcing for multidecadal variations in IOHC since 1960 along with their spatial footprint, both with regard to their depth structure and regional features.

2. Data Sets and Ocean Model Simulations

2.1. Observational and Reanalysis Products

Time series of IOHC were generated by vertically integrating temperature over the upper 700 m and spatially integrating over the Indian Ocean Basin north of 33°S based on the following products: (1) Monthly objectively analyzed subsurface temperature at 1° horizontal resolution for the period 1945–2012 by Ishii et al. (2005), which combines data from the World Ocean Database and Atlas, Centennial in situ Observation Based Estimates (COBE) SST, and Argo profiles. (2) Annual gridded temperature fields from ISAS-15 version 7, entirely based on in situ measurements and covering the period 2002–2015 (Kolodziejczyk et al., 2017). (3) Monthly ocean temperature heat content estimate from Institute of Atmospheric Physics (IAP) at 1° horizontal resolution available for the period 1940–2016 (Cheng et al., 2017). (4) Monthly temperature fields from the European Centre for Medium Range Weather Forecasting Ocean Reanalysis System v5 (ORAS5; Zuo et al., 2019) for the period 1979–2018; ORAS5 uses the Nucleus for European Modeling of the Ocean (NEMO) ocean model v3.4.1 at 0.25° resolution and 75 vertical levels and assimilates SST from HadISST2 and reprocessed in situ profiles from EN4 via 3DVar; and (5) seasonal time series of upper 700-m IOHC from Levitus et al. (2012) for the period 1958–2018.

2.2. NEMO Model Simulations

We use a global ocean model configuration of the NEMO code, v3.6 (Madec, 2016) with a global tripolar ORCA grid at 0.25° horizontal resolution. The vertical grid consists of 46 z-levels with varying layer thickness from 6 m at the surface to 250 m in the deepest levels. The model is forced with the JRA55-do forcing (Tsujino et al., 2018), which builds on the JRA55 atmospheric reanalysis product and adjusted to match observational data sets. Bulk formulas according to Large and Yeager (2009) are used to calculate surface fluxes. All experiments are started from a 30-year-long spin-up (1980–2009) initialized with hydrography from the World Ocean Database (Levitus et al., 1998) and driven by interannually varying atmospheric boundary conditions. The hindcast simulations and the sensitivity runs cover the period 1958–2017, though we restrict our analysis to the 1960–2017 period.

Our study uses three experiments: The hindcast is forced with interannually varying atmospheric boundary conditions. Two sensitivity experiments were performed to distinguish variability due to wind-driven and buoyancy forcing. These two experiments, denoted “buoyancy” and “wind,” were forced without interannual variations of the momentum and buoyancy fluxes, respectively. Further details of the model configuration, experimental setup, and model validation are described in the Supporting Information S1 and in Ryan et al. (2020).

3. Multidecadal IOHC Changes

3.1. Observed IOHC Changes

Upper 700-m IOHC in various observational-based products and our hindcast suggests a notable absence of warming during the period 1960 to the mid-1990s (Figure 1). This is in stark contrast to OHC trends in other tropical ocean basins that exhibit periods of increase throughout much of the second half of the 20th century (e.g., Balmaseda et al., 2013). However, rapid IOHC increases are apparent in all three observational products, the ocean reanalysis, and our hindcast from the late 1990s onwards (Figure 1). The hindcast underestimates the cooler IOHC signal in the 1960s and 1970s compared to the two observational-based products that cover this period (Figure 1). The good agreement between the latter is likely because they both rely on

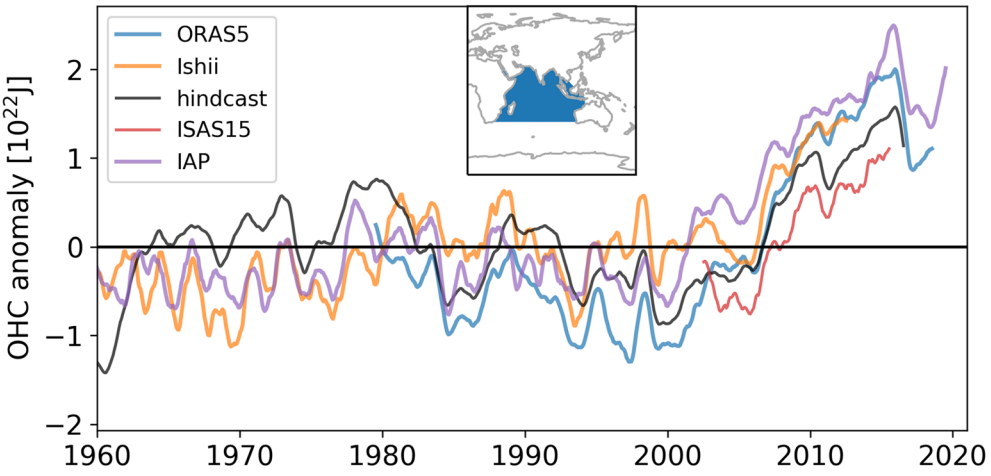

Figure 1. Time series of upper 700 m IOHC anomalies (in 10^{22} J) as 12-month running average for the period 1960–2020 for our ocean model hindcast (black) and three observational-based products: Ishii (1945–2012; Ishii et al., 2005), IAP (1940–2019; Cheng et al., 2017), and ISAS15 (2002–2015; Kolodziejczyket al., 2017). In addition, the ocean reanalysis ORAS5 (1979–2018; Zuo et al., 2019) is shown as well. The blue area in the inset map indicates the region used to derive the IOHC. Note that the base period for the OHC anomalies is taken as 1960–2012 for Ishii, IAP, and the hindcast, while ORAS5 and ISAS15 are relative to a base period 1979–2012 and 2002–2012, respectively, consistent with the data period that they cover.

sparse, yet common, underlying data during this early period, which is also most sensitive to the spatial domain and base period for analysis (for further details see Supporting Information S1). Since the mid-1970s, the hindcast exhibits multidecadal IOHC variations that are within the spread of the observational-based products, and timing and magnitude of the rapid rise in IOHC from the mid-to-late 1990s to 2015 are well reproduced (Figure 1). In the following, we focus on the overall IOHC evolution seen in the hindcast and use sensitivity experiments to highlight the relative contribution of buoyancy and wind stress forcing to IOHC.

3.2. Relative Contributions of Buoyancy and Wind Forcing

We explore the spatial structure and temporal evolution of IOHC changes in Figure 2, showing Indo-Pacific OHC anomalies in 10-year periods between 1960 and 2017 over the upper 700 m for the three experiments. Significance testing of the OHC anomalies used a Monte Carlo approach, as detailed in the Supporting Information S1. The period prior to the mid-1970s was characterized by anomalously high OHC in the western equatorial Pacific, while in the 1980s and 1990s, anomalous cool upper ocean conditions dominated (Figures 2a–2d). In the Indian Ocean, phase reversals of OHC anomalies emerge delayed compared to the western Pacific changes: The signal first appears in the southeastern tropical Indian Ocean, especially pronounced with the warm OHC anomalies in the 1960s/1970s and 2000s and suggestive of the role of enhanced ITF transport, as described for the post-2000 Indian Ocean warming signal (e.g., Gruenburg & Gordon, 2018; Li et al., 2017; Liu et al., 2015; Zhang et al., 2018). The Indo-Pacific upper 700-m OHC spatial patterns and temporal evolution agree well with two observational products available over that time period (Figures S2 and S3).

A complementary analysis of the evolution of the Indo-Pacific upper 700-m OHC in the sensitivity experiments reveals that the OHC anomalies in the hindcast are broadly approximated by a linear addition of the anomalies due to buoyancy and wind-stress forcing, though the match is not perfect (Figures 2s–2x). In the buoyancy experiment, the Indian Ocean is broadly characterized by a general warming trend with largest anomalies in the (sub)tropical eastern basin (Figures 2g–2l). The evolution of OHC in the wind-forced experiment (Figures 2m–2r) instead closely resembles that of the hindcast, including timing and spatial footprint of the OHC reversal in the Pacific and the corresponding emergence of the Indian Ocean signal. The wind experiment shows OHC anomaly patterns with a strong coherence with the IPO, consistent with England et al. (2014) and Maher et al. (2018), i.e., supporting a Pacific trade wind-driven mechanism of

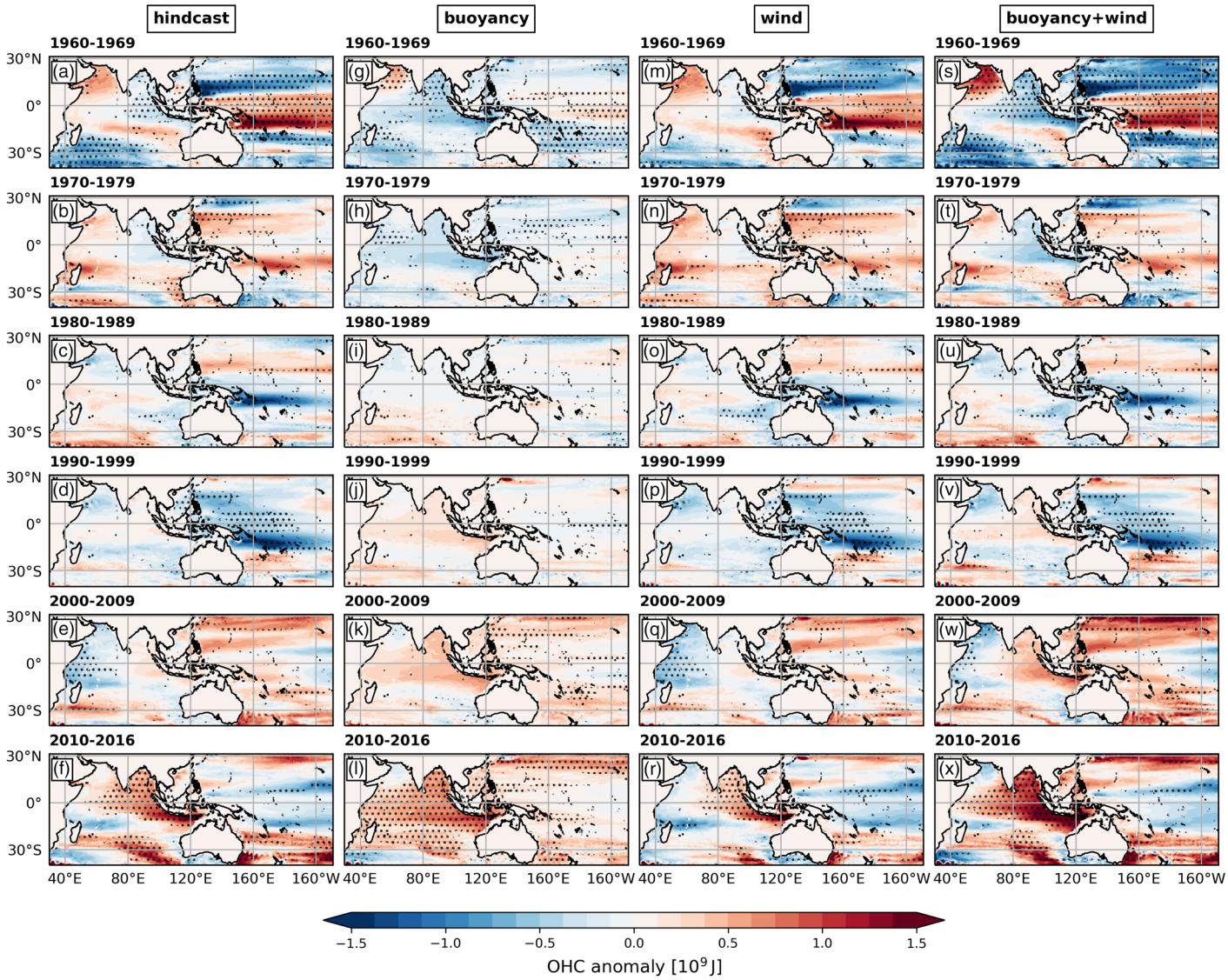

Figure 2. Ocean heat content anomaly (in 10^9 J) in the upper 700 m and averaged for 10-year intervals relative to the analysis period 1960–2017 in the (a–f) ocean model hindcast and sensitivity experiments for (g–l) "buoyancy," (m–r) "wind," as well as a linear addition of the (s–x) "buoyancy" and "wind" sensitivity run. Stippling denotes anomalies significant at the 90% level according to Monte Carlo testing.

spin-up/spin-down of the ITF transport of heat from the Pacific into the Indian Ocean, especially for the positive IPO during the 1980s and 1990s and the post-2000 negative IPO (ending with the most recent IPO phase change in ~2015).

Given the likely role of the IPO in the multidecadal IOHC variations and distinct spatial patterns seen across the Indian Ocean basin, it is informative to explore the temporal evolution of upper 700-m IOHC separately for the eastern and western Indian Ocean in the hindcast and sensitivity experiments (Figure 3). The total IOHC shown in Figure 1 is separated into a western and eastern domain separated along 90°E (cf. Jin, Kwon, Ummenhofer, Seo, Schwarzkopf, et al., 2018). While the buoyancy-forced experiment shows a steady increase in IOHC in the upper 700 m since the 1960s in the east and west, the wind experiment exhibits more multidecadal variability and a decline from the mid-1960s to the late 1990s (Figures 3a and 3e). It should be noted that the OHC anomalies are not scaled to the surface area in the eastern and western domain, which likely contributes to the differences in magnitude. The multidecadal IOHC changes in the hindcast closely

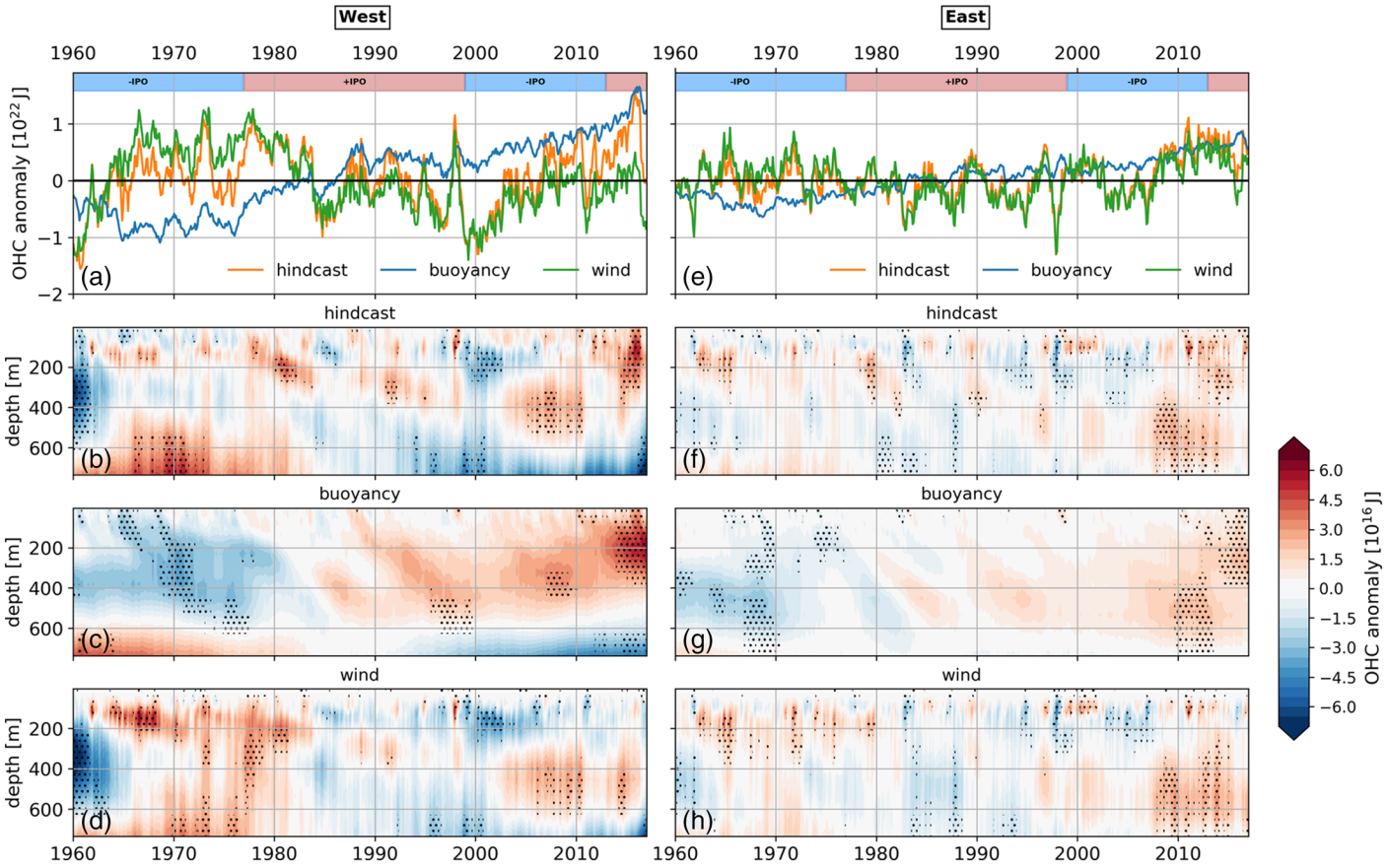

Figure 3. (a and e) Time series of upper 700-m IOHC anomalies (in 10^{22} J) for 1960–2017 for the ocean model simulations spatially averaged over the eastern and western Indian Ocean basin, respectively: hindcast (orange), "buoyancy" (blue), and "wind" (green). (b–h) Hovmöller plots of the temporal evolution of subsurface heat content (in 10^{16} J) spatially averaged over the eastern and western Indian Ocean Basin with depth. The Indian Ocean Basin mask shown in Figure 1 inset is applied and OHC in the west (left) is taken as the region west of 90°E and east (right) as the region east of 90°E. Stippling in (b–h) denotes anomalies significant at the 90% level according to Monte Carlo testing.

resemble those in the wind experiment. In effect, the wind forcing has been compensating the buoyancy-forced IOHC increase from the 1960s through the late 1990s. This appears to be the case in the east and west, though the absolute magnitude of the multidecadal variations of OHC are more prominent in the west than the east (Figures 3a and 3e). Only since 2000 when IOHC in the hindcast starts to rise do both wind and buoyancy forcing contribute positively to IOHC until 2010, when buoyancy seems to dominate until 2015. The sharp post-2000 uptick in IOHC is consistent with that found previously in observations and models (Lee et al., 2015; Maher et al., 2018; Nieves et al., 2015).

Significant IOHC warming continued at least through 2015 and appeared to compensate the concurrent cooling in the upper layer of the Pacific Ocean associated with the hiatus. The strongest contributions to IOHC occur in the 100- to 500-m depth range (Figures 3b–3d and 3f–3h), consistent with observations in Nieves et al. (2015). In the buoyancy-forced run, a period of low subsurface IOHC anomalies is seen during 1960–1980, followed by warm IOHC anomalies since the 1990s, with a shallower warming centered near 200 m and more near-surface anomalies since 2010 (Figures 3c and 3g). Enhanced freshwater input over the Maritime Continent Region and extending into the eastern Indian Ocean appears to be a contributing factor in the last decade, as previously seen to be playing a role in regional warming, circulation, as well as sea level changes in the Southeast Indian Ocean (e.g., Feng et al., 2015; Hu & Sprintall, 2017; Llovel & Lee, 2015). Our results of the relative role of wind and buoyancy forcing during the 2000–2015 period are consistent with Jayasankar et al. (2019), who found the IOHC trend to be dominated by enhanced ITF transport (local surface forcing) during the first (second) half of the hiatus. As such, it appears that local buoyancy and wind forcing post-2010 jointly contributed to the IOHC increase in the eastern Indian Ocean (Figures 2f,

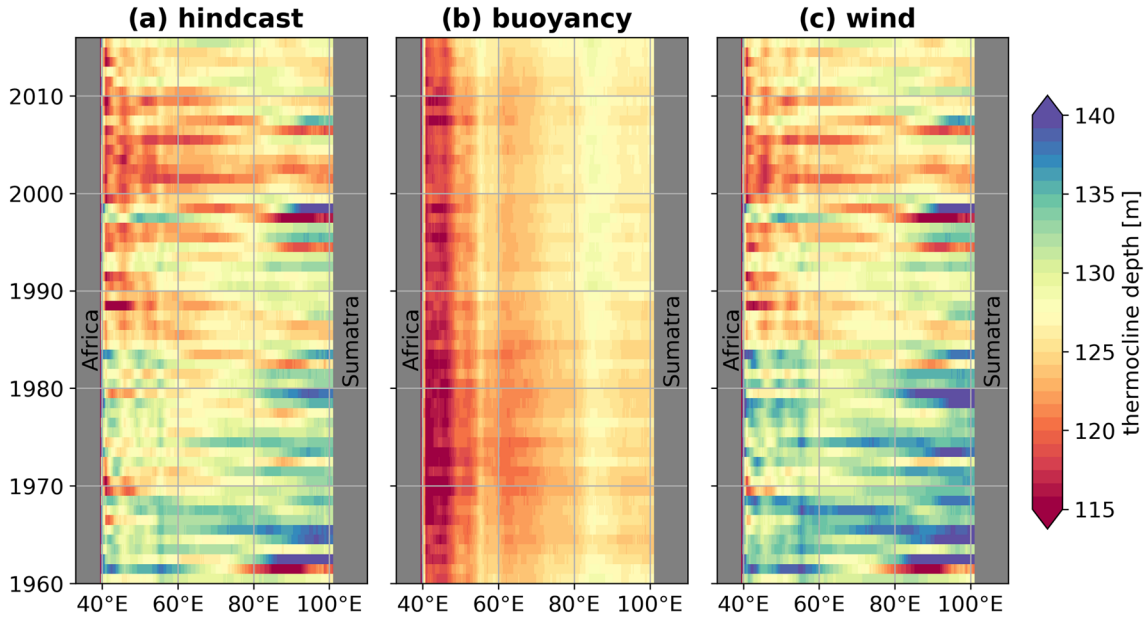

Figure 4. Indian Ocean equatorial cross-section of annual mean thermocline depth (in m; 5°N–5°S) in the ocean model hindcast and sensitivity experiments for (a) hindcast, (b) "buoyancy," and (c) "wind." Thermocline depth is determined as the depth of the 20°C isotherm during the period 1960–2017.

2l, 2r, and 2x). Similar conclusions were reached by Li et al. (2018) when looking at average IOHC and temperature conditions in the top 400 m. However, Figure 3 here demonstrates that buoyancy and wind forcing contribute to temperature changes at different depths within the top 700 m and that wind forcing in particular exhibits a distinct spatiotemporal footprint in the eastern and western Indian Ocean (Figures 3f–3h), implying caution with depth- and basin-wide averages as commonly used in previous studies.

The separation of IOHC into an eastern and western Indian Ocean sector further allows broad partitioning into the components of IOHC influenced by IPO forcing transmitted to the Indian Ocean through the oceanic and atmospheric bridge, respectively, as follows: (1) the eastern IOHC east of 90°E constitutes the component predominantly influenced by the IPO through Pacific wind forcing affecting ITF transport and thermocline adjustments transmitted from the western Pacific through the oceanic connection (Figures 3e–3h); (2) the western IOHC west of 90°E represents the component arising predominantly in response to a remote, IPO-induced shift in the Walker Circulation; this changes local Indian Ocean winds, such that anomalous wind stress and resultant Ekman pumping in the central Indian Ocean west of 90°E can induce westward propagating Rossby waves and associated anomalous OHC (Figures 3b and 3d). This partitioning into an eastern and western IOHC component and links to respective remote and local wind forcing was also highlighted by Jin, Kwon, Ummenhofer, Seo, Schwarzkopf, et al. (2018) using a linear Rossby wave model (cf. their Fig. 9).

The alignment of the timing with IPO-phasing of the IOHC anomalies differs for the western and eastern IOHC: the atmospheric bridge connection that is mediated through shifts in the Walker circulation is relatively quick, as manifest with changes in western IOHC anomalies in the hindcast and wind experiment closely coinciding with IPO phasing (Figure 3a). In contrast, a delay of several years of the emergence of the eastern IOHC signal to IPO phase shifts is seen in the hindcast and wind experiment (Figure 3e), consistent with earlier findings of a 2- to 3-year lag between an ITF-related signal in Makassar Strait and the eastern Indian Ocean (Gruenburg & Gordon, 2018) or a 5- to 6-year delay with the Pacific Decadal Oscillation (Ummenhofer et al., 2017).

4. Equatorial Indian Ocean Thermocline Variations

Variations in the background state of the eastern Indian Ocean thermocline play an important role in modulating the frequency of Indian Ocean Dipole (IOD) events on decadal timescales. The ocean model skillfully

represents Indian Ocean thermocline patterns and variability (cf. Figure S4 and Supplementary Information S1), allowing us to assess equatorial Indian Ocean thermocline variations in response to wind-stress and buoyancy forcing. Cross sections of the annual 20°C isotherm as proxy for equatorial thermocline depth (averaged between 5°N and 5°S) are shown in Figure 4 as a Hovmöller plot for the three experiments. Overall, the 20°C isotherm in the equatorial Indian Ocean has been shoaling since the 1960s, especially pronounced in the west (Figure 4a), consistent with projected shoaling in a warming climate (e.g., Cai et al., 2013). However, substantial multidecadal variability is superimposed on this long-term change, as well as substantial year-to-year variations in thermocline depth exist, more pronounced in the equatorial Indian Ocean east of 80°E. In the buoyancy-forced experiment, an overall deepening of the thermocline can be seen (Figure 4b). On the other hand, the substantial decadal variability in the eastern Indian Ocean thermocline in the hindcast is reproduced by the wind-forced experiment (Figure 4c), echoing thermocline displacements due to equatorial Pacific wind forcing found by Trenary and Han (2013). Interestingly, the shoaling of the western Indian Ocean thermocline (centered at 45°E; Figure 4) seems to be predominantly a response to wind forcing (cf. Figure 3), consistent with earlier findings (e.g., Jin, Kwon, Ummenhofer, Seo, Schwarzkopf, et al., 2018) that IPO-induced wind forcing transmitted via the atmospheric bridge through the zonal Walker circulation modulated western Indian Ocean subsurface variations on decadal timescales. Dong and McPhaden (2016) associated the strong observed interhemispheric SST gradient trends in the Indian Ocean with this mechanism: i.e., post-2000, the IPO-forced shift in the Walker circulation over the Indian Ocean led to downwelling-favorable wind stress curls between 10°S and 20°S deepening the thermocline, while upwelling-favorable winds dominated between the equator and 10°S; this pattern reconciles the strong surface warming as seen in the SST with a progressively shoaling equatorial thermocline and the IOHC changes discussed here.

5. Conclusions

The Indian Ocean sustained robust surface warming over the second half of the 20th century. However, the upper 700-m IOHC reflected a conspicuous absence of a warming trend over the same time period that is in stark contrast to OHC trends in other ocean basins (Balmaseda et al., 2013; Schott et al., 2009). On the other hand, a rapid rise in IOHC and widespread upper ocean warming was observed in the Indian Ocean during the late 1990s to 2015, accounting for a large portion of upper ocean heat gain during the global warming hiatus period (e.g., Lee et al., 2015; Nieves et al., 2015) and likely associated with Pacific wind forcing during the negative IPO phase (England et al., 2014; Kosaka & Xie, 2013; Maher et al., 2018). Here, we used ocean model simulations to disentangle the role of different local and remote atmospheric factors for multidecadal variations in IOHC over the past 60 years by assessing the relative contribution of buoyancy and wind stress forcing on OHC changes regionally and with depth. We demonstrated that multidecadal wind forcing in the second half of the 20th century counteracted increases in IOHC due to buoyancy forcing prior to the 1990s. Both buoyancy and wind forcing contributed positively to the rapid IOHC rise in the early 21st century.

Partitioning IOHC changes into a western and eastern Indian Ocean component, as well as investigating their respective depth structures allows insights into the transmission pathway how IPO-related wind forcing can modulate IOHC changes via both the oceanic and atmospheric bridge: (1) equatorial Pacific wind forcing results in western Pacific OHC and thermocline variations, affecting ITF transport, and further transmitted through the Maritime Continent to the eastern Indian Ocean; (2) local wind forcing over the Indian Ocean arising from IPO-induced shifts in the zonal Walker circulation through the atmospheric bridge across the equatorial Indo-Pacific can locally generate Ekman pumping in the central Indian Ocean that results in thermocline adjustments in the west (Dong & McPhaden, 2016; Jin, Kwon, Ummenhofer, Seo, Schwarzkopf, et al., 2018). Given temporal differences in the speed of transmission of the IPO-induced signal through these two pathways, the temporal evolution of IOHC in the eastern and western Indian Ocean, respectively, is not well aligned in either the hindcast or the wind experiment.

Related multidecadal changes in Indian Ocean thermocline variations, of importance for air-sea coupling and the development of IOD events, were similarly modulated by wind and buoyancy forcing: a progressive shoaling of the western Indian Ocean thermocline in a warming climate (e.g., Cai et al., 2013) coincided with multidecadal modulation by wind forcing throughout the past 60 years and likely accounts for the

low-frequency thermocline variations that can result in clustering of IOD events in certain decades that has been described in the late 20th century (e.g., Annamalai et al., 2005; Ummenhofer et al., 2017) and for previous centuries from the paleoclimate record (Abram et al., 2020).

Data Availability Statement

ORAS5 from ECMWF can be accessed via the Ocean Synthesis Directory, ICDC, University Hamburg (http://icdc.cen.uni-hamburg.de/thredds/catalog/ftpthredds/EASYInit/oras5/catalog.html); Ishii subsurface temperature analyses cab be accessed via the Research Data Archive at NCAR, CISL (https://doi.org/10.5065/Y6CR-KW66); ISAS-15 gridded temperature fields can be accessed online (https://www.seanoe.org/data/00412/52367/); OHC estimate from the Institute for Atmospheric Physics can be accessed online (http://159.226.119.60/cheng/); Levitus global OHC can be accessed via NOAA NCEI (https://www.nodc.noaa.gov/OC5/3M_HEAT_CONTENT/). Derived fields (and visualization scripts to reproduce the figures) are available online (https://hdl.handle.net/20.500.12085/05fb3074-0eaa-11eb-8dd6-c81f66eb46c3); the raw model output is available upon request.

Acknowledgments
We gratefully acknowledge the following observational/reanalysis products: ORAS5 from ECMWF, Ishii subsurface temperature analyses, ISAS-15 gridded temperature fields, OHC estimate from the Institute for Atmospheric Physics, and Levitus global OHC. OGCM simulations were performed at the North-German Supercomputing Alliance (HLRN) and the Computing Centre at Kiel University. This work was supported by the Alexander von Humboldt Foundation (CCU and SR), *The Investment in Science Fund given primarily by WHOI Trustee and Corporation Members* (CCU), *James E. and Barbara V. Moltz Fellowship for climate-related research* (CCU), the ARC Centre of Excellence for Climate Extremes (CE170100023; CCU and MHE), ARC DP150101331 (CCU and MHE), and PW was supported through grant IndoArchipel from the Deutsche Forschungsgemeinschaft (DFG) as part of the Special Priority Program (SPP)-1889"Regional Sea Level Change and Society" (SeaLevel). Raw model output, derived fields, and visualization scripts to reproduce the figures are available online (https://hdl.handle.net/20.500.12085/05fb3074-0eaa-11eb-8dd6-c81f66eb46c3).

References

Abram, N. J., Wright, N. M., Ellis, B., Dixon, B. C., Wurtzel, J. B., England, M. H., et al. (2020). Coupling of Indo-Pacific climate variability over the last millennium. *Nature*, *579*(7799), 385–392. https://doi.org/10.1038/s41586-020-2084-4

Annamalai, H., Potemra, J., Murtugudde, R., & McCreary, J. P. (2005). Effect of preconditioning on the extreme climate events in the tropical Indian Ocean. *Journal of Climate*, *18*(17), 3450–3469. https://doi.org/10.1175/JCLI3494.1

Balmaseda, M. A., Trenberth, K. A., & Källen, E. (2013). Distinctive climate signals in reanalysis of global ocean heat content. *Geophysical Research Letters*, *40*, 1754–1759. https://doi.org/10.1002/grl.50382

Bindoff, N. L., Cheung, W. W. L., Kairo, J. G., Arístegui, J., Guinder, V. A., Hallberg, R., et al. (2019). Changing ocean, marine ecosystems, and dependent communities. In H.-O. Pörtner, et al. (Eds.), *IPCC special report on the ocean and cryosphere in a changing climate* (pp. 447–587). Cambridge, UK: Cambridge University Press.

Cai, W., Zheng, X.-T., Weller, E., Collins, M., Cowan, T., Lengaigne, M., et al. (2013). Projected response of the Indian Ocean Dipole to greenhouse warming. *Nature Geosceince*, *6*(12), 999–1007. https://doi.org/10.1038/NGEO2009

Cheng, L., Trenberth, K., Fasullo, J., Boyer, T., Abraham, J., & Zhu, J. (2017). Improved estimates of ocean heat content from 1960 to 2015. *Science Advances*, *3*, e1601545. https://doi.org/10.1126/sciadv.1601545

Dong, L., & McPhaden, M. J. (2016). Interhemispheric SST gradient trends in the Indian Ocean prior to and during the recent global warming hiatus. *Journal of Climate*, *29*(24), 9077–9095. https://doi.org/10.1175/JCLI-D-16-0130.1

Dong, L., Zhou, T., Dai, A., Song, F., Wu, B., & Chen, X. (2016). The footprint of the inter-decadal Pacific oscillation in Indian Ocean sea surface temperatures. *Scientific Reports*, *6*(1), 21251. https://doi.org/10.1038/srep21251

England, M. H., McGregor, S., Spence, P., Meehl, G. A., Timmermann, A., Cai, W., et al. (2014). Recent intensification of wind-driven circulation in the Pacific and the ongoing warming hiatus. *Nature Climate Change*, *4*(3), 222–227. https://doi.org/10.1038/nclimate2106

Feng, M., Benthuysen, J., Zhang, N., & Slawinski, D. (2015). Freshening anomalies in the Indonesian Throughflow and impacts on the Leeuwin Current during 2010–2011. *Geophysical Research Letters*, *42*, 8555–8562. https://doi.org/10.1002/2015GL06584

Gruenburg, L., & Gordon, A. L. (2018). Variability in Makassar Strait heat flux and its effect on the eastern tropical Indian Ocean. *Oceanography*, *31*, 80–87.

Hu, S., & Sprintall, J. (2017). Observed strengthening of interbasin exchange via the Indonesian seas due to rainfall intensification. *Geophysical Research Letters*, *44*, 1448–1456. https://doi.org/10.1002/2016GL072494

Ishii, M., Kimoto, M., Sakamoto, K., & Iwasaki, S. (2005). Subsurface temperature and salinity analyses. Research Data Archive at the National Center for Atmospheric Research, Computational and Information Systems Laboratory. https://doi.org/10.5065/Y6CR-KW66

Jayasankar, T., Eldho, T. I., Ghosh, S., & Murtugudde, R. (2019). Assessment of the interannual variability of local atmospheric and ITF contribution to the subsurface heat content of southern tropical Indian Ocean in GECCO2 and ORAS4 using ROMS. *Global and Planetary Change*, *181*, 102974. https://doi.org/10.1016/j.gloplacha.2019.05.014

Jin, X., Kwon, Y.-O., Ummenhofer, C. C., Seo, H., Kosaka, Y., & Wright, J. S. (2018). Distinct mechanisms of decadal subsurface heat content variations in the eastern and western Indian Ocean modulated by tropical Pacific SST. *Journal of Climate*, *31*(19), 7751–7769. https://doi.org/10.1175/JCLI-D-18-0184.1

Jin, X., Kwon, Y.-O., Ummenhofer, C. C., Seo, H., Schwarzkopf, F. U., Biastoch, A., et al. (2018). Influences of Pacific climate variability on decadal subsurface ocean heat content variations in the Indian Ocean. *Journal of Climate*, *31*, 4154–4174.

Kolodziejczyk, N., Prigent-Mazella, A., & Fabienne, G. (2017). ISAS-15 temperature and salinity gridded fields. SEANOE. https://doi.org/10.17882/52367

Kosaka, Y., & Xie, S.-P. (2013). Recent global-warming hiatus tied to equatorial Pacific surface cooling. *Nature*, *501*(7467), 403–407. https://doi.org/10.1038/nature12534

Large, W., & Yeager, S. (2009). The global climatology of an interannually varying air-sea flux data set. *Climate Dynamics*, *33*(2–3), 341–364. https://doi.org/10.1007/s00382-008-0441-3

Lee, S.-K., Park, W., Baringer, M. O., Gordon, A. L., Huber, B., & Liu, Y. (2015). Pacific origin of the abrupt increase in Indian Ocean heat content during the warming hiatus. *Nature Geoscience*, *8*(6), 445–449. https://doi.org/10.1038/ngeo2438

Levitus, S., Antonov, J. I., Boyer, T. P., Baranova, O. K., Garcia, H. E., Locarnini, R. A., et al. (2012). World ocean heat content and thermosteric sea level change (0–2000 m), 1955–2010. *Geophysical Research Letters*, *39*, L10603. https://doi.org/10.1029/2012GL051106

Levitus, S., Boyer, T. P., Conkright, M. E., O'Brien, T., Antonov, J., Stephens, C., et al. (1998). World ocean database 1998, volume 1: Introduction. Tech. rep, NOAA Atlas NESDIS 18, U.S. Government Printing Office, Washington, D.C.

Li, Y., Han, W., Hu, A., Meehl, G. A., & Wang, F. (2018). Multidecadal changes of the upper Indian Ocean heat content during 1965-2016. *Journal of Climate*, *31*(19), 7863–7884. https://doi.org/10.1175/JCLI-D-18-0116.1

Li, Y., Han, W., Wang, F., Zhang, L., & Duan, J. (2020). Vertical wtructure of the upper-Indian Ocean thermal variability. *Journal of Climate*, *33*(17), 7233–7253. https://doi.org/10.1175/JCLI-D-19-0851.1

Li, Y., Han, W., & Zhang, L. (2017). Enhanced decadal warming of the southeast Indian Ocean during the recent global surface warming slowdown. *Geophysical Research Letters*, *44*, 9876–9884. https://doi.org/10.1002/2017GL075050

Liu, Q.-Y., Feng, M., Wang, D., & Wijffels, S. (2015). Interannual variability of the Indonesian Throughflow transport: A revisit based on 30 year expendable bathythermograph data. *Journal Geophysical Research: Oceans*, *120*, 8270–8282. https://doi.org/10.1002/2015JC011351

Llovel, W., & Lee, T. (2015). Importance and origin of halosteric contribution to sea level change in the southeast Indian Ocean during 2005–2013. *Geophysical Research Letters*, *42*, 1148–1157. https://doi.org/10.1002/2014GL062611

Luo, J.-J., Sasaki, W., & Masumoto, Y. (2012). Indian Ocean warming modulates Pacific climate change. *Proceedings of the National Academy of Sciences*, *109*(46), 18,701–18,706. https://doi.org/10.1073/pnas.1210239109

Madec, G. (2016). NEMO ocean engine 2014: Tech. rep, Note Pôle Model. Inst. Pierre-Simon Laplace, Paris, 27.

Maher, N., England, M. H., Sen Gupta, A., & Spence, P. (2018). Role of Pacific trade winds in driving ocean temperatures during the recent slowdown and projections under a wind trend reversal. *Climate Dynamics*, *51*(1–2), 321–336. https://doi.org/10.1007/s00382-017-3923-3

Nieves, V., Willis, J. K., & Patzert, W. C. (2015). Recent hiatus caused by decadal shift in Indo-Pacific heating. *Science*, *349*(6247), 532–535. https://doi.org/10.1126/science.aaa4521

Ryan, S., Ummenhofer, C. C., Gawarkiewicz, G., Wagner, P., Scheinert, M., Biastoch, A., & Böning, C. W. (2020). Depth structure of Ningaloo Niño/Niña events and associated drivers. *Journal of Climate*, 1–65. https://doi.org/10.1175/JCLI-D-19-1020.1

Schott, F. A., Xie, S.-P., & McCreary, J. P. (2009). Indian Ocean variability and climate variability. *Reviews of Geophysics*, *47*, RG1002. https://doi.org/10.1029/2007RG000245

Schwarzkopf, F. U., & Böning, C. W. (2011). Contribution of Pacific wind stress to multi-decadal variations in upper-ocean heat content and sea level in the tropical South Indian Ocean. *Geophysical Research Letters*, *38*, L12602. https://doi.org/10.1029/2011GL047651

Trenary, L. L., & Han, W. (2013). Local and remote forcing of decadal sea level and thermocline depth variability in the South Indian Ocean. *Journal of Geophysical Research: Oceans*, *118*, 381–398. https://doi.org/10.1029/2012JC008317

Tsujino, H., Urakawa, S., Nakano, H., Small, R. J., Kim, W. M., Yeager, S. G., et al. (2018). JRA-55 based surface dataset for driving ocean-sea-ice models (JRA55-do). *Ocean Modelling*, *130*, 79–139. https://doi.org/10.1016/j.ocemod.2018.07.002

Ummenhofer, C. C., Biastoch, A., & Böning, C. W. (2017). Multi-decadal Indian Ocean variability linked to the Pacific and implications for preconditioning Indian Ocean Dipole events. *Journal of Climate*, *30*(5), 1739–1751. https://doi.org/10.1175/JCLI-D-16-0200.1

Vialard, J. (2015). Hiatus heat in the Indian Ocean. *Nature Geoscience*, *8*(6), 423–424. https://doi.org/10.1038/ngeo2442

Zhang, Y., Feng, M., Du, Y., Phillips, H. E., Bindoff, N. L., & McPhaden, M. J. (2018). Strengthened Indonesian Throughflow drives decadal warming in the southern Indian Ocean. *Geophysical Research Letters*, *45*, 6167–6175. https://doi.org/10.1029/2018GL078265

Zuo, H., Balmaseda, M. A., Tietsche, S., Mogensen, K., & Mayer, M. (2019). The ECMWF operational ensemble reanalysis–analysis system for ocean and sea ice: A description of the system and assessment. *Ocean Science*, *15*(3), 779–808. https://doi.org/10.5194/os-15-779-2019

References From the Supporting Information

Beal, L. M., Vialard, J., Roxy, M. K., Ravichandran, M., McPhaden, M. J., Feng, M., et al. (2019). Executive summary. IndOOS-2: A roadmap to sustained observations of the Indian Ocean for 2020-2030. CLIVAR-4/2019, GOOS-237, I-VIII pp. https://doi.org/10.36071/clivar.rp.4-1.2019

Duteil, O., Böning, C. W., & Oschlies, A. (2014). Variability in subtropical-tropical cells drives oxygen levels in the tropical Pacific Ocean. *Geophysical Research Letters*, *41*, 8926–8934. https://doi.org/10.1082/2014GL061774

Feng, M., Biastoch, A., Böning, C., Caputi, N., & Meyers, G. (2008). Seasonal and interannual variations of upper ocean heat balance off the west coast of Australia. *Journal of Geophysical Research*, *113*, C12025. https://doi.org/10.1029/2008JC004908

Feng, M., Böning, C., Biastoch, A., Behrens, E., Weller, E., & Masumoto, Y. (2011). The reversal of the multi-decadal trends of the equatorial Pacific easterly winds, and the Indonesian Throughflow and Leeuwin Current transports. *Geophysical Research Letters*, *38*, L11604. https://doi.org/10.1029/2011GL047291

Gordon, A. L., Sprintall, J., van Aken, H. M., Susanto, D., Wijffels, S., Molcard, R., et al. (2010). The Indonesian Throughflow during 2004–2006 as observed by the INSTANT program. *Dynamics of Atmospheres and Oceans*, *50*(2), 115–128. https://doi.org/10.1016/j.dynatmoce.2009.12.002

Han, W., Vialard, H., McPhaden, M. J., Lee, T., Masumoto, Y., Feng, M., & de Ruijter, W. P. M. (2014). Indian Ocean decadal variability: A review. *Bulletin of the American Meteorological Society*, *97*, 1679–1703.

Lübbecke, J., Böning, C. W., & Biastoch, A. (2008). Variability in the subtropical-tropical cells and its effect on near-surface temperature of the equatorial Pacific: A model study. *Ocean Science*, *4*(1), 73–88. https://doi.org/10.5194/os-4-73-2008

Sprintall, J., Wijffels, S. E., Molcard, R., & Jaya, I. (2009). Direct estimates of the Indonesian Throughflow entering the Indian Ocean: 2004–2006. *Journal of Geophysical Research*, *114*, C07001. https://doi.org/10.1029/2008JC005257

Stewart, K. D., Kim, W., Urakawa, S., Hogg, A. M., Yeager, S., Tsujino, H., et al. (2020). JRA55-do-based repeat year forcing datasets for driving ocean–sea-ice models. *Ocean Modelling*, *147*, 101557. https://doi.org/10.1016/j.ocemod.2019.101557

Ummenhofer, C. C., Schwarzkopf, F. U., Meyers, G. A., Behrens, E., Biastoch, A., & Böning, C. W. (2013). Pacific Ocean contribution to the asymmetry in eastern Indian Ocean variability. *Journal of Climate*, *26*(4), 1152–1171. https://doi.org/10.1175/JCLI-D-11-00673.1

Yuan, X., Ummenhofer, C. C., Seo, H., & Su, Z. (2020). Relative contributions of heat flux and wind stress on the spatiotemporal upper-ocean variability in the tropical Indian Ocean. *Environmental Research Letters*, *15*, 084047. https://doi.org/10.1088/1748-9326/ab9f7f